Phase transitions in phospholipid monolayers: Statistical model at the pair approximation

F. O. de Oliveira[*] and M. N. Tamashiro[†]

Instituto de Física "Gleb Wataghin", Universidade Estadual de Campinas (UNICAMP), Rua Sérgio Buarque de Holanda, 777, Cidade Universitária, Campinas SP, 13083-859, Brazil

(Received 24 September 2018; published 31 January 2019)

A Langmuir film, consisting of a phospholipid monolayer at the air-water interface, was modeled as a two-dimensional lattice gas corresponding to a ternary mixture of water molecules (w), ordered-chain lipids (o), and disordered-chain lipids (d). The statistical problem is formulated in terms of a spin-1 model, in which the disordered-chain lipid states possess a high degenerescence $\omega \gg 1$, and was termed Doniach lattice gas (DLG). Motivated by some open questions in the analysis of the DLG model at the mean-field approximation (MFA) [Phys. Rev. E **90**, 052705 (2014)], we have reconsidered it at the pair-approximation level by solving the model on a Cayley tree of coordination z. The attractors of the corresponding discrete-map problem are associated with the thermodynamic solutions on the Bethe lattice (the central region of an asymptotically infinite Cayley tree). To check the thermodynamic stability of the possible phases, the grand-potential density was obtained by the method proposed by Gujrati [Phys. Rev. Lett. **74**, 809 (1995)]. In general, the previous MFA results are confirmed at the pair-approximation level, but a novel staggered phase, overlooked in the MFA analysis, was found when the condition $\epsilon_{\rm wd} > \frac{1}{2}(\epsilon_{\rm ww} + \epsilon_{\rm dd})$ is satisfied, where ϵ_{xy} represents the nearest-neighbor intermolecular interactions between single-site states x and y. Model parameters obtained by fitting to experimental data for the two most commonly studied zwitterionic phospholipids, 1,2-dimyristoyl-sn-glycero-3-phosphocholine (DMPC) and 1,2-dipalmitoyl-sn-glycero-3-phosphocholine (DPPC), yield phase diagrams consistent with the phase transitions observed on Langmuir films of the same lipids under isothermal compression, which present a liquid-condensed to a liquid-expanded first-order transition line ending at a critical point.

DOI: 10.1103/PhysRevE.99.012147

I. INTRODUCTION

Amphiphile molecules, in particular, phospholipids, are essential constituents of membrane cells of all living organisms [1]. These are usually comprised by unilamellar vesicles that are formed by a mixture of lipids self-assembled in the form of a bilayer matrix, onto which other macromolecules, e.g., proteins and cholesterol, are aggregated in order to keep its biological function [2]. Bilayers are spontaneously formed in water dispersions of phospholipids, with the hydrophilic polar heads binding to the surrounding water molecules through hydrogen bonds, while the hydrophobic fatty-acid chains core prevents contact with the aqueous medium. A related system, where intermolecular interactions between amphiphiles and water molecules play a role, are the so-called Langmuir films [3,4], which are formed when a single amphiphile layer resides at the air-water interface. In this case, the polar heads arrange in such a way that they keep immersed in the aqueous solution, while the hydrocarbon chains point towards the air phase. Here the monolayer specific area (area per amphiphile molecule) can be controlled by application of an external lateral pressure.

When Langmuir films are isothermally compressed, one observes that, for a specific coexistence surface pressure Π^* that depends on temperature T and on the amphiphile molecule, there are abrupt variations in the monolayer specific area, associated with phase transitions [3,4]. In general, two transitions of this type are observed, commonly called gas-liquid expanded (G-LE) and liquid expanded-liquid condensed (LE-LC) transitions, in analogy to the gas-liquid transition in three-dimensional simple fluids. After years of controversy about the nature of these phase transitions [5–8], it is recognized today that they would be indeed discontinuous (first-order) [3,4], displaying thus an associated latent heat. Due to their discontinuous character, it is possible that these transitions might disappear above a critical point, specific for each amphiphile molecule, associated with a well-defined critical surface pressure Π_c and critical temperature T_c. On increased compression, a second-order transition, liquid condensed-solid crystalline (LC-SC), may be observed, which will not be considered in this work. For higher surface pressures, the monolayer eventually expands to three dimensions and may even collapse [9].

Different statistical lattice models have been proposed to describe phase transitions in zwitterionic phospholipids [10,11], for which the hydrophilic head group, although polar, has a null net charge. Nagle [12] proposed to evaluate the hydrophobic-chain entropy through exact enumeration of the possible configurations, by mapping the problem on a dimer model. Doniach [13] adopted a simpler approach, introducing a model that can be mapped into the two-dimensional

[*]Present address: Instituto de Física, Universidade de São Paulo (USP), Rua do Matão, 1371, Cidade Universitária, São Paulo SP, 05508-090, Brazil; foliva@usp.br

[†]mtamash@ifi.unicamp.br

spin-1/2 ferromagnetic Ising model [14–17]. In the Doniach model [13], each lipid molecule may be in one of two possible states: an ordered (gel-like) state (o) or a disordered (liquid-like) state (d). The disordered state displays a high degenerescence $\omega \gg 1$, attributed to the rotamers of the lipid chains in this state. This simplified model predicts a thermotropic first-order transition, which may be associated with the LE-LC transition. In order to reproduce the experimental density gap observed in the LE-LC transition, Doniach imposed, in an *ad hoc* fashion, distinct areas per molecule for the two lipid states. Although this model and its extensions [18–20] were successful to describe some features of the main transition of zwitterionic phospholipids, the Doniach model [13] is unfit to describe the G-LE transition, which may be observed in some monolayer experiments [3]. Also, the model does not allow lipid-density fluctuations, by its own formulation, due to the fixed *ad hoc* areas assumed for the two lipid states. This limitation represents a severe shortcoming of the Doniach model, as lipid-density fluctuations constitute a crucial ingredient to characterize some features of ionic-lipid systems [21,22].

In order to address these drawbacks of the Doniach model [13], the Doniach lattice gas (DLG) has been proposed [23]. The DLG model represents an extension of the Doniach model that allows lipid-density fluctuations, by introducing a new vacant state (w), corresponding to lattice sites filled by water molecules. In fact, this additional state is not properly a vacant (passive) state but also interacts with both remaining lipid states already defined in the Doniach model [13], being thus equivalent to a ternary mixture of pure components (w, o, d). The DLG model can be written in terms of spin-1 variables [23], representing an extension of a ternary-mixture model [24,25], in which one of the states (d, disordered lipid chain) displays a high degenerescence $\omega \gg 1$.

In the original DLG model proposal [23], the authors settled for a general mean-field-approximation (MFA) analysis of the model predictions, together with Monte Carlo simulations for some points of interest in the phase diagram. In particular, the authors did not explore model parameters that imply the existence of a critical point at the end of the LE-LC first-order transition line, observed for some lipid systems. As we are essentially working with a diluted model, we have decided to treat it at a pair-approximation level, which is more accurate than the fully connected MFA Hamiltonian to describe critical behavior. To implement the pair approximation, we employ a Bethe-Gujrati [26] lattice scheme, which provides a direct way to obtain the self-consistent grand potential at the pair-approximation level, as well as allows one to easily detect staggered or modulated phases. In fact, this formulation indicated the existence of a staggered phase, overlooked in the previous MFA analysis [23], making it necessary to treat the DLG model at the pair approximation on a bipartite lattice. An explicit comparison of theoretical predictions at the pair-approximation level with isothermal compression experiments [27] is done elsewhere [28].

The purpose of the current study is then to reanalyze the DLG model, briefly reviewed in Sec. II, under the framework of the pair approximation, implemented via the Bethe-Gujrati lattice scheme in Sec. III. Our main results are presented in Sec. IV, displaying the possible types of phase diagrams predicted at the pair approximation. In particular, in comparison to previous MFA results [23], two new types of phase diagrams were found, which display a staggered phase, overlooked in the MFA analysis. Some final comments are presented in Sec. V. Three appendices provide details for a few technical points. The critical conditions are derived in Appendix A. Appendix B presents the pair-approximation equations of state and associated grand-potential density for a bipartite lattice, necessary to properly characterize the staggered phase. Appendix C discusses the possible types of phase diagrams, based on asymptotic expressions of the limiting spin-1/2 Ising models, in analogy to the Appendix of Ref. [23].

TABLE I. Nearest-neighbor pair states, spin representation, and associated intramolecular and intermolecular energies. The single-site states are as follows: water (w), ordered-chain lipid (o), and disordered-chain lipid (d).

Pair state	Spin-1 representation	$\epsilon_x + \epsilon_y$	ϵ_{xy}
ww	0 0	$2\epsilon_{\rm w}$	$\epsilon_{\rm ww}$
wo	0 +	$\epsilon_{\rm w} + \epsilon_{\rm o}$	$\epsilon_{\rm wo}$
wd	0 −	$\epsilon_{\rm w} + \epsilon_{\rm d}$	$\epsilon_{\rm wd}$
oo	+ +	$2\epsilon_{\rm o}$	$\epsilon_{\rm oo}$
od	+ −	$\epsilon_{\rm o} + \epsilon_{\rm d}$	$\epsilon_{\rm od}$
dd	− −	$2\epsilon_{\rm d}$	$\epsilon_{\rm dd}$

II. DEFINITION OF THE DLG MODEL

The DLG model [23] represents a three-component lattice gas, where the $N_{\rm t}$ sites of the monolayer, modeled as a regular two-dimensional lattice with lattice parameter a_0 and coordination z, can be occupied either by a cluster of water molecules or a phospholipid head-group. In turn, the fatty-acid chains attached to the lipid head groups may be in two possible states, ordered or disordered, the latter being characterized by a degenerescence $\omega \gg 1$. We label these three single-site states as (w, o, d) for sites occupied by water, ordered-chain lipid, and disordered-chain lipid, respectively. Besides the single-site intramolecular energies $-\epsilon_x$, $x \in$ (w, o, d), nearest-neighbors sites interact by short-ranged attractive pairwise interactions $-\epsilon_{xy}$, $x \in$ (w, o, d), $y \in$ (w, o, d). Table I summarizes the possible nearest-neighbors configurations and their contribution to the total energy of the system, as well as the spin-1 representation to be introduced in the statistical model.

It is possible to describe the effective Hamiltonian of the model in the grand-canonical ensemble in terms of spin-1 variables [23–25,28], with the single-site states (w, o, d) at lattice site i represented by the spin variables $s_i = 0, +1, -1$, respectively,

$$\mathcal{H}(\{s_i\}) = -J\sum_{(i,j)} s_i s_j - K\sum_{(i,j)} s_i^2 s_j^2 - \frac{L}{2}\sum_{(i,j)} s_i s_j (s_i + s_j) - \mu_{\rm eff}\sum_i s_i^2 - H\sum_i s_i - E_0, \quad (1)$$

where the (i, j) sums run over all distinct pairs of z nearest neighbors on the two-dimensional lattice and the effective parameters (J, K, L, H, E_0) are fixed and can be expressed

[28] in terms of the lower-level intra- and intermolecular energies (ϵ_x, ϵ_{xy}),

$$J = \frac{1}{4}(\epsilon_{oo} + \epsilon_{dd} - 2\epsilon_{od}), \tag{2}$$

$$K = \frac{1}{4}(\epsilon_{oo} + \epsilon_{dd} + 4\epsilon_{ww} + 2\epsilon_{od} - 4\epsilon_{wo} - 4\epsilon_{wd}), \tag{3}$$

$$L = \frac{1}{2}(\epsilon_{oo} - \epsilon_{dd} - 2\epsilon_{wo} + 2\epsilon_{wd}), \tag{4}$$

$$H = \frac{z}{2}(\epsilon_{wo} - \epsilon_{wd}) + \frac{1}{2}(\epsilon_o - \epsilon_d), \tag{5}$$

$$E_0 = N_t\left(\frac{z}{2}\epsilon_{ww} + \epsilon_w + \mu_w\right). \tag{6}$$

Because of the additional constraint in the DLG model of fixed total area $A = N_t a_0$, only the difference of the chemical potentials of lipids μ_{lip} and water μ_w is relevant as a thermodynamic field in the effective chemical potential,

$$\mu_{eff} = \mu_{lip} - \mu_w - \frac{z}{2}(2\epsilon_{ww} - \epsilon_{wo} - \epsilon_{wd}) - \frac{1}{2}(2\epsilon_w - \epsilon_o - \epsilon_d). \tag{7}$$

We will consider the water chemical potential μ_w and lower-level energies (ϵ_x, ϵ_{xy}) as fixed, and take the effective chemical potential μ_{eff} as a proxy for the lipid chemical potential μ_{lip}.

The effective Hamiltonian (1) represents a generalization of the Blume-Emery-Griffiths (BEG) model [29], whose extended version including cubic (dipole-quadrupole) terms, but without degenerescence ($\omega = 1$), has been proposed in the study of tricritical behavior in simple fluids [30], binary mixtures [25,31], and ternary mixtures [24,25]. One should also mention that there are a few spin-1 models proposed in the literature to describe lipid monolayers [32–37], which, however, predict second-order (continuous) phase transitions, in disagreement with the current hypothesis that they represent, in fact, discontinuous (first-order) transitions [5–8].

The associated grand-canonical partition function then reads

$$\Xi(T, A = N_t a_0, \mu_{eff}, H) = \sum_{\{s_i\}} \omega^{N_d(\{s_i\})} \exp\left[-\beta\mathcal{H}(\{s_i\})\right], \tag{8}$$

with $\beta \equiv (k_B T)^{-1}$, k_B is the Boltzmann constant, T is the absolute temperature, and N_d is the total number of disordered-chain lipids in the monolayer,

$$N_d = \frac{1}{2}\sum_i s_i(s_i - 1). \tag{9}$$

It will be convenient to introduce the dimensionless parameters

$$j \equiv \beta J, \quad k \equiv \beta K, \quad \ell \equiv \beta L, \quad \mu \equiv \beta\mu_{eff}, \quad h \equiv \beta H, \tag{10}$$

in terms of which one may write the grand-canonical partition function

$$\Xi = e^{\beta E_0}\sum_{\{s_i\}}\left[\prod_i \omega^{\frac{1}{2}s_i(s_i-1)} e^{\mu s_i^2 + h s_i}\right] \times \exp\left\{\sum_{(i,j)}\left[j s_i s_j + k s_i^2 s_j^2 + \frac{\ell}{2} s_i s_j (s_i + s_j)\right]\right\}. \tag{11}$$

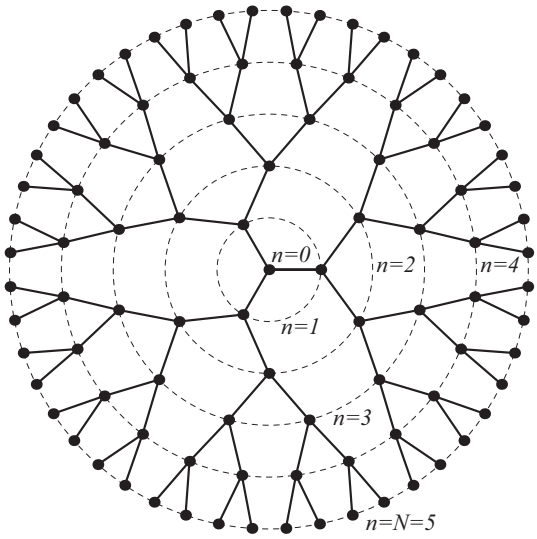

FIG. 1. A Cayley tree of coordination $z = 3$, composed of a zeroth ($n = 0$) site surrounded by $N = 5$ generations of sites. Each surface site (at generation $n = N = 5$) has a single nearest neighbor lying at the preceding generation $n = 4$, while all interior sites ($n < N$) have equally z nearest neighbors.

The grand-partition function, Eq. (11), will be evaluated at the pair-approximation level using the method described in the next section. Henceforth the reference energy will be set to $E_0 \equiv 0$, by taking the full water-filled state as the reference state. It will be also postulated that the only difference between the ordered-chain and the disordered-chain lipid states is of entropic nature, through ω, so that $\epsilon_{wo} = \epsilon_{wd}$ and $\epsilon_o = \epsilon_d$, implying thus $h = 0$, which will be assumed later in the numerical calculations. However, all analytical calculations will carry a nonvanishing h in order to keep the results general.

III. DLG MODEL ON THE BETHE LATTICE AND GUJRATI'S METHOD

The Cayley tree (CT) is a cycle-free graph. It is obtained by defining a central ("root" or "zeroth") site ($n = 0$) and z edges emanating from this central site to the first generation ($n = 1$) of sites. Beyond this first generation, each site is connected to a branch consisting of $z - 1$ edges. When this process is repeated N times, we have a CT of coordination z and N generations, as depicted in Fig. 1 for $z = 3$ and $N = 5$. In a CT, the number N_s of surface sites increases exponentially, as does the number $N_b \equiv N_t - N_s$ of sites in the bulk. In the thermodynamic limit the ratio of surface-to-bulk sites *is not negligible,* instead converging to $\lim_{N\to\infty} N_s/N_b = z - 2$. This gives rise to a thermodynamic behavior extremely dependent on the boundary conditions [38–42] that is of mostly mathematical interest but perhaps of little application in the realm of physics. Although it seems to exist some controversy about the proper mathematical nomenclature to be used [43], because a Bethe lattice (BL) would be, by definition, *infinite*, whereas a CT would be *always finite*, we adopt the standard equivalence [38,39] acknowledged between a BL and the interior of an *asymptotically infinite* CT *far enough*

from its surface, which yields approximated solutions of the equivalent problem formulated on a regular lattice, generally identical to the traditional Bethe-Peierls approximation (BPA) [44–47]. Based on this standard interpretation and with the aid of Gujrati's method [26], later we will also be able to obtain the thermodynamically consistent grand potential on the BL, from which the BPA equations of state can be obtained. Although Ref. [43] critically reviewed this equivalence, unfortunately it did not offer an alternative to Gujrati's method for the calculation of the self-consistent BL thermodynamical potential.

We begin calculating the grand-partition function of the system, Eq. (11), by exploiting the self-similar structure of the graph. If we remove the central site s_0, the higher generations of the graph are split into z independent, self-similar tree branches. Therefore, the grand-partition function $\Xi_{0,N}$ of the whole CT, with root spin indexed 0 and surface generation indexed N, reads

$$\Xi_{0,N} = \sum_{s_0} \Xi_0(s_0) = \Xi_0(+) + \Xi_0(-) + \Xi_0(0), \tag{12}$$

with the partial partition functions of the whole tree $\Xi_0(s_0)$, for fixed central spin s_0, given by

$$\Xi_0(s_0) = \omega^{\frac{1}{2}s_0(s_0-1)} e^{\mu s_0^2 + h s_0} \times \left[\sum_{s_1} e^{j s_0 s_1 + k s_0^2 s_1^2 + \frac{\ell}{2} s_0 s_1 (s_0 + s_1)} Q_1(s_1) \right]^z, \tag{13}$$

written in terms of the partial partition functions $Q_1(s_1)$ of a tree branch starting at generation $n = 1$, with the innermost site (root of the branch) fixed at spin s_1.

On the other hand, for any site besides the root ($n \neq 0$), if we remove any single site s_n, then we split the higher generations of the graph into $z - 1$ independent tree branches. We can use this property to obtain a recurrence relation involving the partial partition functions $Q_{n-1}(s)$ and $Q_n(s)$ associated with successive generations. The partial traces over the $z - 1$ tree branches on the generation n yields

$$Q_{n-1}(s) = \omega^{\frac{1}{2}s(s-1)} e^{\mu s^2 + h s} \times \left[\sum_{s_n} e^{j s s_n + k s^2 s_n^2 + \frac{\ell}{2} s s_n (s + s_n)} Q_n(s_n) \right]^{z-1}. \tag{14}$$

The crucial difference between Eqs. (13) and (14) are the exponents z and $z - 1$, originated from the distinct number of connected outermost tree branches for the root and peripheral sites of the CT. Eventually, having traced over all N generations of the CT, we are left with the boundary condition

$$Q_N(s) = \omega^{\frac{1}{2}s(s-1)}\, e^{\mu s^2 + h s}, \tag{15}$$

because the surface sites at generation $n = N$ interact only with the sites of the penultimate generation $N - 1$.

While the partial partition functions $\{Q_n(s)\}$ themselves are recursive and, in the thermodynamic limit $N \to \infty$, technically divergent, we can use their ratios to obtain truncated pseudoaverages at the branch root of generation $n \geqslant 1$, while it is still disconnected from the innermost $n - 1$ generations of the CT,

$$m_n \equiv \frac{\sum_s s\, Q_n(s)}{\sum_{s'} Q_n(s')} = \frac{Q_n(+) - Q_n(-)}{Q_n(0) + Q_n(+) + Q_n(-)} = \frac{x_n - y_n}{1 + x_n + y_n}, \tag{16}$$

$$q_n \equiv \frac{\sum_s s^2 Q_n(s)}{\sum_{s'} Q_n(s')} = \frac{Q_n(+) + Q_n(-)}{Q_n(0) + Q_n(+) + Q_n(-)} = \frac{x_n + y_n}{1 + x_n + y_n}, \tag{17}$$

where we have introduced auxiliary variables (x_n, y_n), defined by the ratios

$$x_n \equiv \frac{Q_n(+)}{Q_n(0)} = \frac{q_n + m_n}{2(1 - q_n)}, \tag{18}$$

$$y_n \equiv \frac{Q_n(-)}{Q_n(0)} = \frac{q_n - m_n}{2(1 - q_n)}. \tag{19}$$

In terms of them, the recurrence relations (14) between the $\{Q_n(s)\}$ can be rewritten as

$$x_{n-1} = e^{\mu + h} X^{z-1}(x_n, y_n), \tag{20}$$

$$y_{n-1} = \omega e^{\mu - h}\, Y^{z-1}(x_n, y_n), \tag{21}$$

$$X(x_n, y_n) = \frac{1 + e^{j+k+\ell} x_n + e^{k-j} y_n}{1 + x_n + y_n}, \tag{22}$$

$$Y(x_n, y_n) = \frac{1 + e^{k-j} x_n + e^{j+k-\ell} y_n}{1 + x_n + y_n}, \tag{23}$$

or, in a form more convenient to perform numerical calculations, in terms of the bounded pseudoaverages (m_n, q_n), $-1 \leqslant m_n \leqslant 1, 0 \leqslant q_n \leqslant 1$,

$$m_{n-1} = \frac{e^h X^{z-1}(m_n, q_n) - \omega e^{-h}\, Y^{z-1}(m_n, q_n)}{e^{-\mu} + e^h X^{z-1}(m_n, q_n) + \omega e^{-h}\, Y^{z-1}(m_n, q_n)}, \tag{24}$$

$$q_{n-1} = \frac{e^h X^{z-1}(m_n, q_n) + \omega e^{-h}\, Y^{z-1}(m_n, q_n)}{e^{-\mu} + e^h X^{z-1}(m_n, q_n) + \omega e^{-h}\, Y^{z-1}(m_n, q_n)}, \tag{25}$$

$$X(m_n, q_n) = 1 - q_n + \frac{1}{2} e^{j+k+\ell}(q_n + m_n) + \frac{1}{2} e^{k-j}(q_n - m_n), \tag{26}$$

$$Y(m_n, q_n) = 1 - q_n + \frac{1}{2} e^{k-j}(q_n + m_n) + \frac{1}{2} e^{j+k-\ell}(q_n - m_n). \tag{27}$$

The above recurrence relations, for a given set of fixed parameters $(j, k, \ell, \mu, h, \omega, z)$, defines a two-dimensional dynamical discrete map that may converge to an attractor, depending on the initial choice of boundary conditions at the surface (m_N, q_N), even though, for a rigorous CT, the boundary conditions are fully determined by Eq. (15). In

this work, we have observed, in the investigated range of parameters, the presence of single fixed points as well as two-cycle fixed points (orbits of period two), associated with a staggered thermodynamic phase. If the generation label subscripts are dropped from the recursive formulas, then they can also be interpreted as a pair of simultaneous coupled nonlinear transcendental equations. Simultaneously solving these equations can lead to numerically unstable and stable solutions, the latter being identical to the single fixed points of the discrete map.

Beginning with a set of different initial conditions (m_N, q_N), we proceed to iterate the map and, after a sufficient number of steps for convergence to the desired or arbitrary accuracy, we obtain one or more stable fixed points for the same set of fixed parameters $(j, k, \ell, \mu, h, \omega, z)$. When the recurrence relations have converged, we can drop the subscripts and consider $(x_n, y_n) \to (x, y)$ or $(m_n, q_n) \to (m, q)$. Now we consider the root of the tree at $n = 0$. As already pointed out, the fundamental difference in calculating the partial traces on a branch root at peripheral sites and the partition function on the tree root at the central site is that they have, respectively, $z - 1$ and z nearest neighbors. With this in mind, we can obtain the values for (x_0, y_0) at the central site or, equivalently, (m_0, q_0), which are the true, *bona fide,* thermal averages on the BL, via Boltzmann weights in the grand-canonical ensemble,

$$x_0 \equiv \frac{\Xi_0(+)}{\Xi_0(0)} = e^{\mu+h} X^z(x, y) = x X(x, y), \tag{28}$$

$$y_0 \equiv \frac{\Xi_0(-)}{\Xi_0(0)} = \omega e^{\mu-h} Y^z(x, y) = y Y(x, y), \tag{29}$$

$$\begin{aligned} m_0 \equiv \langle s_0 \rangle &= \frac{1}{\Xi_{0,N}} \sum_{s_0} s_0 \, \Xi_0(s_0) = \frac{x_0 - y_0}{1 + x_0 + y_0} \\ &= \frac{4m(1-q) + e^{j+k+\ell}(q+m)^2 - e^{j+k-\ell}(q-m)^2}{4(1-q^2) + e^{j+k+\ell}(q+m)^2 + e^{j+k-\ell}(q-m)^2 + 2e^{k-j}(q^2-m^2)}, \end{aligned} \tag{30}$$

$$\begin{aligned} q_0 \equiv \langle s_0^2 \rangle &= \frac{1}{\Xi_{0,N}} \sum_{s_0} s_0^2 \, \Xi_0(s_0) = \frac{x_0 + y_0}{1 + x_0 + y_0} \\ &= \frac{4q(1-q) + e^{j+k+\ell}(q+m)^2 + e^{j+k-\ell}(q-m)^2 + 2e^{k-j}(q^2-m^2)}{4(1-q^2) + e^{j+k+\ell}(q+m)^2 + e^{j+k-\ell}(q-m)^2 + 2e^{k-j}(q^2-m^2)}. \end{aligned} \tag{31}$$

These thermal averages are associated with the fractions of sites filled with ordered-chain and disordered-chain lipids in the system, ϕ_o and ϕ_d, and the lipid surface density σ for the DLG model under the BPA,

$$\phi_o \equiv \frac{\langle N_o \rangle}{N_t} = \frac{1}{2}(q_0 + m_0), \tag{32}$$

$$\phi_d \equiv \frac{\langle N_d \rangle}{N_t} = \frac{1}{2}(q_0 - m_0), \tag{33}$$

$$\sigma \equiv \frac{\langle N_{lip} \rangle}{N_t} = \frac{\langle N_o + N_d \rangle}{N_t} = \frac{\langle N_{lip} \rangle a_0}{A} = q_0, \tag{34}$$

where N_{lip} is the total number of lipid molecules, irrespective of whether the associated fatty-acid chains are ordered or disordered; N_d is the total number of disordered-chain lipids in the monolayer, given by Eq. (9); while N_o is the total number of ordered-chain lipids in the monolayer,

$$N_o = \frac{1}{2} \sum_i s_i (s_i + 1). \tag{35}$$

While this works for the order parameters, the departure from self-similarity imposed by this last step requires a different approach for calculating the BL grand-potential density, which is needed to determine the thermodynamically stable solution in the case of numerical costability of multiple stable fixed points and, therefore, to locate possible first-order phase transitions. Fortunately, there is a simple method to obtain, via the BL formalism, an analytical expression for the thermodynamic potential in the pair approximation. It was originally proposed by Gujrati [26], and it is quite reliable. It is derived from noting that a single CT with root at generation 0 and surface at generation N has the same number of surface sites as $z - 1$ CTs with surface also at generation N but root at generation 1. The difference in the *total* number of sites is two, while the difference in the number of *bonds* is z. If we consider that the free energy per site depends on the generation n, we can effectively subtract the contribution from the surface to obtain the average free energy per site between the zeroth and the first generation. That is precisely $z/2$ times the average free energy *per bond* in the BPA. Without delving into details of the calculation, we obtain the pair-approximation grand-potential density per site on the BL,

$$\begin{aligned} \beta\psi(T, \mu, h) &= -\frac{1}{2} \lim_{N\to\infty} \ln \frac{\Xi_{0,N}}{\Xi_{1,N}^{z-1}} = -\frac{1}{2} \lim_{N\to\infty} \ln \frac{\Xi_{0,N}}{\Xi_{0,N-1}^{z-1}} \\ &= \ln(1-q) + \frac{1}{2}(z-2) \ln \Big[1 - q^2 \\ &\quad + \frac{1}{4} e^{j+k+\ell}(q+m)^2 + \frac{1}{4} e^{j+k-\ell}(q-m)^2 \\ &\quad + \frac{1}{2} e^{k-j}(q^2 - m^2) \Big], \end{aligned} \tag{36}$$

which is consistent with the BPA equations of state, Eqs. (30) and (31), as can be checked by the canonical thermodynamic

relations

$$m_0 = -\left(\frac{\partial\beta\psi}{\partial h}\right)_{T,\,\mu}, \quad q_0 = -\left(\frac{\partial\beta\psi}{\partial\mu}\right)_{T,\,h}. \tag{37}$$

Therefore, (m_0, q_0) are truly the thermodynamically conjugate variables to the fields $(H, \mu_{\rm eff})$ of the effective Hamiltonian, Eq. (1). Although this method seems to contradict the fact that the CT and the BL are *fundamentally* different, we can assert that, in the BL, every site can be labeled as being s_0, the root of a CT. In this fashion, we impose the translational invariance inherent to the BL such that, in this approximation, the interactions happen between nearest neighbors that are all identical s_0 sites. This is equivalent to saying that the grand-potential density is the same for every site, and there is no generation labeling, because *any* site can be chosen to be the central one.

For the two-cycle fixed point, we need to reformulate the whole problem on a bipartite lattice, splitting the system into two interpenetrating sublattices a and b in a similar way as performed for the BEG model with repulsive biquadratic interactions [48]. There will be two associated fields for each sublattice, h_a, h_b, μ_a, and μ_b, conjugated to the magnetizations and quadrupole moments m_a^0, m_b^0, q_a^0, and q_b^0. This demands some more cumbersome algebra but is otherwise straightforward, and the final expressions are given in Appendix A. Interestingly enough, the grand-potential densities obtained either with the central site on sublattice a, or on sublattice b, have exactly the same expressions.

The original DLG paper [23] presented some (μ, T) MFA phase diagrams—see, e.g., Figs. 4, 7, and 12 of Ref. [23]—where there is a G-LE first-order transition line ending at a critical point. As the critical behavior was not the main focus of that work, besides the estimates obtained by an asymptotic analysis, the position of the critical points were just obtained numerically. Furthermore, they did not consider a set of model parameters that yields a critical point at the end of the LE-LC first-order transition line. However, to accurately obtain the (μ_c, T_c) coordinates of possible critical points, we must calculate partial derivatives of the proper thermodynamic potential [24,49], in this case, the inverse Legendre transform of the grand potential,

$$\beta\varphi(T, \mu, m_0) \equiv \beta\psi[T, \mu, h(T, \mu, m_0)] + m_0\, h(T, \mu, m_0), \tag{38}$$

in which the intensive field h is replaced by its conjugated order parameter m_0. As the derivation of the critical conditions for the DLG model on the BL is somewhat cumbersome and requires some rather technical details [24,49], we presented it on Appendix B.

IV. RESULTS: PHASE DIAGRAMS AND THE STAGGERED PHASE

To present the numerical results, instead of using the previously defined dimensionless parameters (j, k, ℓ, μ, h), it is more convenient to use dimensionless parameters scaled to the bilinear coupling J,

$$t \equiv \frac{1}{j} = \frac{1}{\beta J}, \quad \bar{k} \equiv \frac{K}{J} = \frac{k}{j}, \quad \bar{\ell} \equiv \frac{L}{J} = \frac{\ell}{j},$$
$$\bar{\mu} \equiv \frac{\mu_{\rm eff}}{J} = \frac{\mu}{j}, \quad \bar{h} \equiv \frac{H}{J} = \frac{h}{j} = 0. \tag{39}$$

First, one has to take into account the finite lattice coordination z on MFA and BPA to be able to more closely compare the phase diagrams generated by both approximations. Therefore, a meaningful comparison between the two approximations requires working with normalized parameters in order to enforce the equivalence between MFA and BPA results. Although the MFA analysis of Ref. [23] was not cast in a form independent of the lattice coordination z—in fact, it was chosen and fixed the coordination $z = 4$—a rigorous universal MFA invariant form can be directly obtained by plotting their results using the dimensionless variables $(t, \bar{\mu})$ scaled to the lattice coordination z, $(t, \bar{\mu}) \to (t/z, \bar{\mu}/z)$, the same applying, approximately, to the BPA results. One expects, at least for higher coordinations z, that the topology of the MFA phase diagrams is retained under BPA for similar values of the effective couplings.

Furthermore, when comparing the phase diagrams of the DLG model obtained here by the BPA with those found by the MFA [23], it is important to bear in mind that the MFA overestimates the stability of the ordered phases, because it neglects thermal fluctuations. In other words, MFA always leads to higher first-order phase transitions and critical temperatures than exact calculations, with the BPA performing better than MFA, yielding values in between the exact and MFA results. More concretely, the spin-1/2 ferromagnetic Ising model critical temperatures under the MFA and the BPA [39,44–47],

$$t_c^{\rm MFA} = z,$$
$$t_c^{\rm BPA} = \frac{1}{\operatorname{arctanh}\left(\frac{1}{z-1}\right)} = \frac{2}{\ln\left(\frac{z}{z-2}\right)} \approx \begin{cases} 2.8854\ (z=4), \\ 4.9326\ (z=6), \end{cases} \tag{40}$$

are both higher than the exact values for the two-dimensional square [15] and triangular [50] lattices,

$$t_c^{\rm exact}(\square, z=4) = \frac{2}{\operatorname{arcsinh} 1} = \frac{-2}{\ln\left(\sqrt{2}-1\right)} \approx 2.2692, \tag{41}$$

$$t_c^{\rm exact}(\triangle, z=6) = \frac{2}{\operatorname{arcsinh}\left(1/\sqrt{3}\right)} = \frac{4}{\ln 3} \approx 3.6410. \tag{42}$$

In the Appendix of Ref. [23] the authors provided asymptotic results, in terms of the spin-1/2 Ising model, that relate their MFA predictions to Monte Carlo calculations. This analysis can be also applied for the BPA, provided one takes into account a correction factor $\phi(z)$ given by the ratio of the critical temperatures of the spin-1/2 ferromagnetic Ising model under BPA and MFA,

$$\phi(z) \equiv \frac{t_c^{\rm BPA}}{t_c^{\rm MFA}} = \frac{2}{z\ln\left(\frac{z}{z-2}\right)}, \tag{43}$$

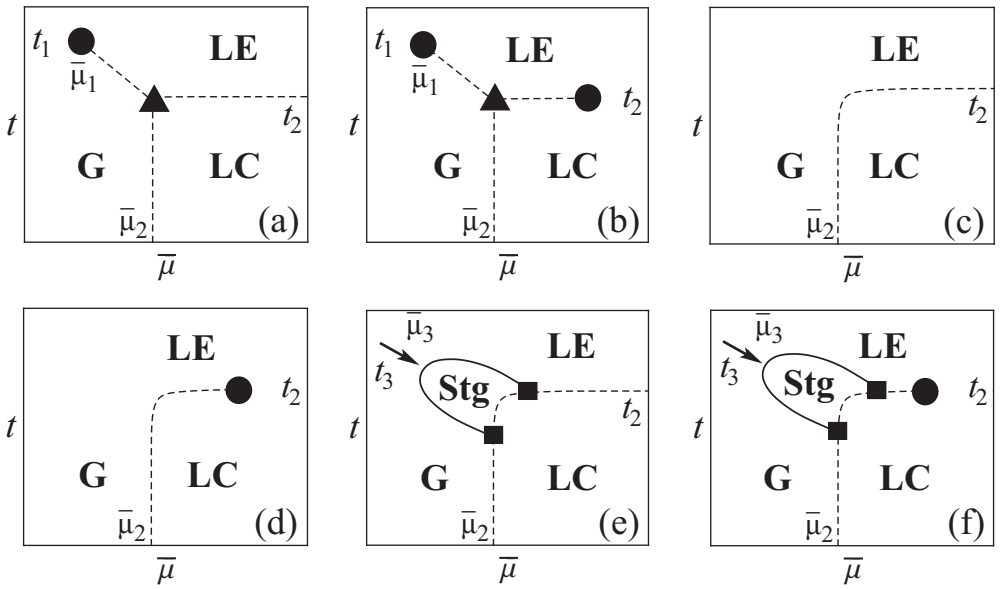

FIG. 2. Temperature t versus effective chemical potential $\bar{\mu}$ typical phase diagrams obtained for the DLG model under BPA for $\bar{h} = 0$. Solid and dashed lines represent, respectively, second-order and first-order phase transitions. Special points of the phase diagrams are indicated by symbols: triple points (▲), critical points (●), and critical-end points (■). Although all these phase-diagram topologies are also presented at MFA, only cases (a) and (c) were detailed in Ref. [23]. Besides the standard (G, LE, LC) phases, there is a staggered (Stg) phase, which requires a division of the system in two interpenetrating sublattices for a proper treatment, not implemented in the previous MFA analysis [23], that being the reason why the Stg phase has not been found there. Estimates of the representative values $(\bar{\mu}_1, \bar{\mu}_2, \bar{\mu}_3, t_1, t_2, t_3)$ are explicitly given in Appendix C. The arrows point to the apices of the oblique lobes that delimit the Stg phase, associated with the parameters $(\bar{\mu}_3, t_3)$, obtained by mapping them into the Néel points of the corresponding effective spin-1/2 Ising antiferromagnet.

and is detailed in Appendix C. Figure 2 displays typical $\bar{h} = 0$ phase-diagram topologies for the DLG model under BPA, which are consistent with this asymptotic analysis adapted to BPA (see Appendix C).

Figure 3 displays the phase diagrams corresponding to the two most commonly studied zwitterionic phospholipids in the literature, 1,2-dimyristoyl-sn-glycero-3-phosphocholine (DMPC) and 1,2-dipalmitoyl-sn-glycero-3-phosphocholine (DPPC). The model parameters were chosen to fit experimental isothermal compression data [27], and the procedure is presented in detail elsewhere [28]. In particular, for both lipids, we have found only a LE-LC first-order transition line ending at a critical point, in agreement with the experimental observations.

However, the onset of a staggered (Stg) phase when $L > J + K$, which implies $\epsilon_{wd} > \frac{1}{2}(\epsilon_{ww} + \epsilon_{dd})$, associated with types (e) and (f) of phase diagrams shown in Fig. 2, was overlooked in Ref. [23]. Figure 4 displays the profile of the lipid order parameter m_0, obtained for the DLG model by the

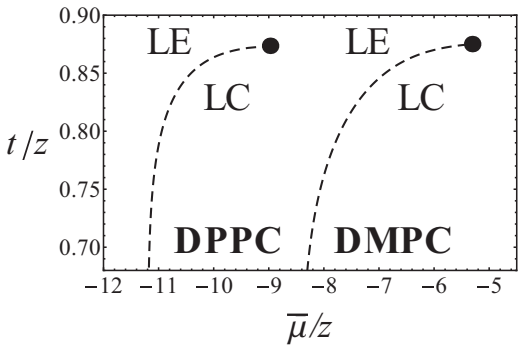

FIG. 3. Temperature t/z versus effective chemical potential $\bar{\mu}/z$ phase diagrams obtained for the DLG model under BPA using numerical parameters obtained by fitting experimental isothermal compression data [27] corresponding to two specific phospholipids [28]: DPPC ($z = 6$, $\omega = 3.5 \times 10^5$, $\bar{h} = 0$, $\bar{\ell} = 11.17619$, $\bar{k} = 10.20970$) and DMPC ($z = 6$, $\omega = 4 \times 10^4$, $\bar{h} = 0$, $\bar{\ell} = 9.30161$, $\bar{k} = 6.51200$). The dashed lines represent the LE-LC first-order transition, ending at a critical point (●).

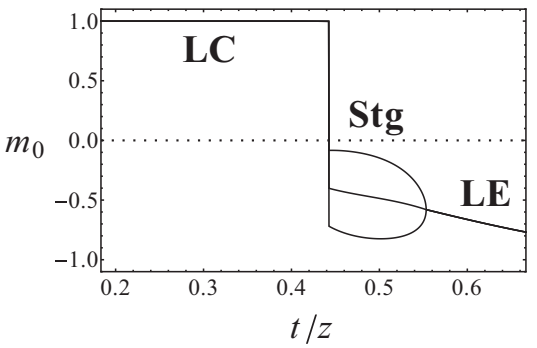

FIG. 4. Profile of the lipid order parameter m_0 as a function of the dimensionless temperature t/z, obtained for the DLG model under BPA, for $z = 6$, $\omega = 4 \times 10^4$, $\bar{h} = 0$, $\bar{\ell} = 5.8$, $\bar{k} = 2$, and $\bar{\mu}/z = -4$. For the Stg phase both the average order parameter m_0, as well as the sublattice order parameters m_a^0 and m_b^0, are shown. There are two phase transitions: a LC-Stg first-order transition around $t/z \approx 0.44$ and a Stg-LE second-order transition around $t/z \approx 0.55$.

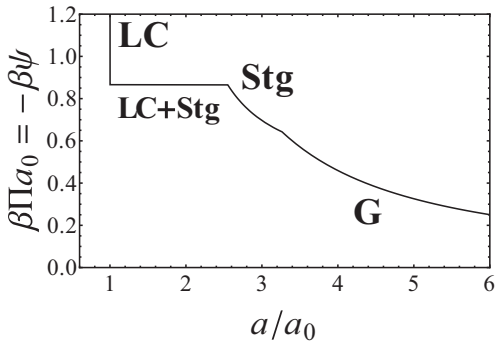

FIG. 5. Dimensionless surface-pressure isotherm, given by the Euler equation $\beta\Pi a_0 = -\beta\psi$, versus dimensionless lipid area $a/a_0 = \sigma^{-1} = q_0^{-1}$, obtained for the DLG model under BPA, for $z = 6$, $\omega = 4 \times 10^4$, $\bar{h} = 0$, $\bar{\ell} = 5.8$, $\bar{k} = 2$, and $t/z = 0.44$. There are two phase transitions: a LC-Stg first-order transition associated with a horizontal coexistence plateau for $a_0 < a \lessapprox 2.6a_0$ and a Stg-G second-order transition around $a \approx 3.3a_0$, which can be better visualized by the inverse isothermal compressibility κ^{-1} in Fig. 6.

BPA, as a function of the dimensionless temperature t/z for a fixed set of parameters that yields a phase diagram of type (e). One may notice the occurrence of two phase transitions as the temperature is raised: a LC-Stg first-order transition, followed by a Stg-LE second-order transition.

The monolayer surface pressure Π and its associated isothermal compressibility κ read

$$\Pi = -\frac{\psi}{a_0}, \quad \kappa = -\frac{1}{a}\left(\frac{\partial a}{\partial \Pi}\right)_T, \tag{44}$$

and are plotted in Figs. 5 and 6 as a function of the area per lipid $a = a_0/q_0$ for the same fixed set of parameters used in Fig. 4 that leads to a Stg phase. In this case, fixing the temperature and varying the lipid density $\sigma = q_0 = a_0/a$, the monolayer undergoes a LC-Stg first-order transition at higher lipid densities, followed by a Stg-G second-order transition at lower lipid densities.

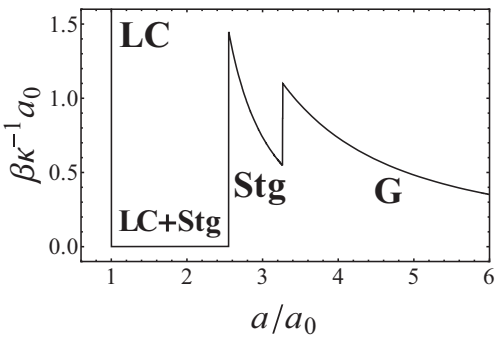

FIG. 6. Inverse dimensionless isothermal compressibility $\beta\kappa^{-1}a_0$ versus dimensionless lipid area $a/a_0 = \sigma^{-1} = q_0^{-1}$, obtained for the DLG model under BPA, for $z = 6$, $\omega = 4 \times 10^4$, $\bar{h} = 0$, $\bar{\ell} = 5.8$, $\bar{k} = 2$, and $t/z = 0.44$. The Stg-G second-order transition is associated with a jump of κ^{-1}, while the horizontal plateau associated with the LC-Stg coexistence along the first-order transition yields a vanishing κ^{-1}.

One should bear in mind, however, that when considering the DLG model on a two-dimensional triangular lattice ($z = 6$), in fact a bipartite-lattice splitting is not possible: See our final comments in Sec. V about the spin-1/2 Ising antiferromagnet on a triangular lattice in a magnetic field [51–58]. Most likely the Stg single-lobe phase region on the $t \times \bar{\mu}$ phase diagrams, predicted for bipartite lattices, must be replaced by a double-lobe structure, when a proper treatment on a tripartite lattice is performed. Though compelling, it is beyond the scope of the present work further investigation of this issue.

V. CONCLUDING REMARKS

We revisited the DLG model at the pair-approximation level through the Bethe-Gujrati method, implemented via calculations on a Cayley tree. The original paper where the DLG model was introduced treated it at the MFA level [23]. In general, our pair-approximation results are consistent with the MFA predictions. However, a novel staggered phase, overlooked in the MFA analysis [23], was found for some range of interaction parameters, namely for $\epsilon_{wd} > \frac{1}{2}(\epsilon_{ww} + \epsilon_{dd})$, when the limiting spin-1/2 Ising model that describes the G-LE transition becomes *antiferromagnetic*. We have checked that this staggered phase would be indeed obtained, even at the MFA level, when a proper bipartite-lattice analysis is performed.

One should mention, however, that the ordered state of the spin-1/2 Ising antiferromagnet on a triangular lattice ($z = 6$) in the presence of a magnetic field is highly nontrivial due to geometric frustration and cannot be simply described by a bipartite-lattice staggered state [51–58]. A proper treatment should consider the DLG model, for example, on the Husimi cactus [59], which displays the appropriate sublattice geometry compatible with the low-temperature ordered phase. The study of this nontrivial and important question deserves further investigation. However, it is beyond the scope of the present work.

Due to the complex structure of the low-temperature ordered phase of the spin-1/2 Ising antiferromagnet on a triangular lattice in the presence of a magnetic field, we suggest that a proper treatment of the novel Stg phase on a tripartite triangular-lattice monolayer and its further correspondence to bilayers, might be related to the so-called pretransition [60] and its associated *ripple* phase [61–70], which are observed in experiments with lipid bilayers, both for the zwitterionic, as well as for the ionic cases.

In a companion paper [28], we perform an explicit comparison of the theoretical pair-approximation predictions obtained here, with isothermal compression experimental measurements [27] for the two most commonly studied zwitterionic phospholipids in the literature, DMPC and DPPC. In particular, in both cases the G phase is consistently absent and there is only a LE-LC first-order transition line ending at a critical point.

ACKNOWLEDGMENTS

The authors thank H. S. Guidi and V. B. Henriques for fruitful discussions. F.O. acknowledges financial support

from the Brazilian agencies Coordination for the Improvement of Higher Education Personnel (CAPES, Grant No. 1186359/2013) and National Council for Scientific and Technological Development (CNPq, Grant No. 142249/2017-3). The National Institute of Science and Technology Complex Fluids (INCT-FCx) is also acknowledged, sponsored by the Brazilian agencies CNPq (Grant No. 465259/2014-6), São Paulo Research Foundation (FAPESP, Grant No. 2014/50983-3), and CAPES (Grant No. 88887.136373/2017-00).

APPENDIX A: CRITICAL CONDITIONS

In this Appendix, we obtain the two additional conditions that define the critical points. The procedure to locate the critical points is presented in Refs. [24,49] and can be expressed in terms of the vanishing $h^{(1)} = h^{(2)} = 0$ of the two first partial derivatives of the field h conjugated to m_0, for constant μ and T,

$$h^{(n)} \equiv \left(\frac{\partial^n h}{\partial m_0^n}\right)_{\mu,T} = \left(\frac{\partial h^{(n-1)}}{\partial m_0}\right)_{\mu,T}, \quad h^{(0)} \equiv h. \tag{A1}$$

Henceforth, in this Appendix, we will omit the constant T condition in the partial derivatives. We must note that the fields (h, μ) were given in terms of the auxiliary variables (x, y) or (m, q),

$$e^{2h} = \frac{\omega x}{y}\left[\frac{Y(x,y)}{X(x,y)}\right]^{z-1} = \frac{\omega(q+m)}{q-m}\left[\frac{Y(m,q)}{X(m,q)}\right]^{z-1}, \tag{A2}$$

$$e^{2\mu} = \frac{xy[X(x,y)Y(x,y)]^{1-z}}{\omega} = \frac{q^2-m^2}{4\omega(1-q)^2}[X(m,q)Y(m,q)]^{1-z}, \tag{A3}$$

and not directly in terms of their thermodynamically conjugated order parameters (m_0, q_0). Therefore, it is convenient to rewrite the critical conditions $h^{(1)} = h^{(2)} = 0$ in terms of the auxiliary variables (m, q),

$$h^{(1)} \equiv \left(\frac{\partial h}{\partial m_0}\right)_\mu = \left(\frac{\partial h}{\partial m}\right)_\mu \left(\frac{\partial m}{\partial m_0}\right)_\mu \equiv \eta^{(1)}\left(\frac{\partial m_0}{\partial m}\right)_\mu^{-1} = 0, \tag{A4}$$

$$h^{(2)} \equiv \left(\frac{\partial h^{(1)}}{\partial m_0}\right)_\mu = \frac{\partial}{\partial m}\left[\eta^{(1)}\left(\frac{\partial m}{\partial m_0}\right)_\mu\right]_\mu \left(\frac{\partial m}{\partial m_0}\right)_\mu = \left(\frac{\partial \eta^{(1)}}{\partial m}\right)_\mu \left(\frac{\partial m}{\partial m_0}\right)_\mu^2 \equiv \eta^{(2)}\left(\frac{\partial m_0}{\partial m}\right)_\mu^{-2} = 0. \tag{A5}$$

If we guarantee that the transformation $(m_0, q_0) \to (m, q)$ is not singular,

$$\left(\frac{\partial m_0}{\partial m}\right)_\mu = \frac{\partial(m_0,\mu)}{\partial(m,q)}\frac{\partial(m,q)}{\partial(m,\mu)} \neq \infty, \tag{A6}$$

which is generally the case, then the critical conditions $h^{(1)} = h^{(2)} = 0$ imply also $\eta^{(1)} = \eta^{(2)} = 0$, conditions that are simpler to evaluate, because they are partial derivatives with respect to the auxiliary variable m, instead with respect to the order parameter m_0.

For the sake of a clean notation, we denote the partial derivatives of the fields (h, μ) through subscripts,

$$\begin{aligned}
h_m &\equiv \left(\frac{\partial h}{\partial m}\right)_q, \quad h_q \equiv \left(\frac{\partial h}{\partial q}\right)_m, \quad h_{2m} \equiv \left(\frac{\partial h_m}{\partial m}\right)_q, \\
h_{2q} &\equiv \left(\frac{\partial h_q}{\partial q}\right)_m, \quad h_{mq} \equiv \left(\frac{\partial h_m}{\partial q}\right)_m, \\
\mu_m &\equiv \left(\frac{\partial \mu}{\partial m}\right)_q, \quad \mu_q \equiv \left(\frac{\partial \mu}{\partial q}\right)_m, \quad \mu_{2m} \equiv \left(\frac{\partial \mu_m}{\partial m}\right)_q, \\
\mu_{2q} &\equiv \left(\frac{\partial \mu_q}{\partial q}\right)_m, \quad \mu_{mq} \equiv \left(\frac{\partial \mu_m}{\partial q}\right)_m,
\end{aligned} \tag{A7}$$

leading to

$$\eta^{(1)} \equiv \left(\frac{\partial h}{\partial m}\right)_\mu = \frac{\partial(h,\mu)}{\partial(m,q)}\frac{\partial(m,q)}{\partial(m,\mu)} = \frac{h_m\mu_q - h_q\mu_m}{\mu_q} = 0, \tag{A8}$$

$$\begin{aligned}
\eta^{(2)} &\equiv \left(\frac{\partial^2 h}{\partial m^2}\right)_\mu = \left(\frac{\partial \eta^{(1)}}{\partial m}\right)_\mu = \frac{\partial(\eta^{(1)},\mu)}{\partial(m,q)}\frac{\partial(m,q)}{\partial(m,\mu)} \\
&= h_{2m} - \frac{2h_{mq}\mu_m}{\mu_q} + \frac{2h_q\mu_m\mu_{mq}}{\mu_q^2} + h_{2q}\left(\frac{\mu_m}{\mu_q}\right)^2 \\
&\quad - \frac{h_q}{\mu_q}\left[\mu_{2m} + \left(\frac{\mu_m}{\mu_q}\right)^2\mu_{2q}\right] = 0.
\end{aligned} \tag{A9}$$

Condition (A8) defines the spinodal lines, which represent the limit of stability of the possible phases, and can be expressed by the solution of the quadratic equation

$$\kappa_2\, e^{2k} + \kappa_1 e^k + \kappa_0 = 0, \tag{A10}$$

$$\kappa_2 = e^{-j}[(z-1)q + 2 - z]\{[ze^{-2j} - e^{2j}(z-2)](q^2-m^2) + e^{\ell}(q+m)^2 + e^{-\ell}(q-m)^2\}, \tag{A11}$$

$$\begin{aligned}
\kappa_1 = (1-q)\{&e^{\ell}(q+m)[m(z-1)^2 \\
&- z[(z-4)q+2] - 3q + 4] - e^{-\ell}(q-m) \\
&\times[m(z-1)^2 + z[(z-4)q+2] + 3q - 4] \\
&- 2e^{-2j}[m^2(z-1)^2 + (1-z^2)q^2 - 2q]\},
\end{aligned} \tag{A12}$$

$$\kappa_0 = 4(1-q)^2 e^{\ell}[(z-1)q + 1]. \tag{A13}$$

The additional condition for criticality, Eq. (A9), represents the meeting of the spinodal lines of different solutions at a critical point, associated with the end of a first-order phase transition line, and can be combined with Eq. (A8) to yield

$$\begin{aligned}
&(2h_q\mu_{mq} + h_{2q}\mu_m - h_m\mu_{2q})h_m \\
&\quad = (2h_{mq}\mu_m + h_q\mu_{2m} - h_{2m}\mu_q)h_q.
\end{aligned} \tag{A14}$$

It is readily obvious that the explicit equation in terms of the model parameters and auxiliary variables should be quite extensive, because of the several partial derivatives involved. Nonetheless, it is straightforwardly obtainable with the aid

of any mathematical software that can perform symbolic manipulations and can then be solved numerically provided some care is taken in choosing suitable starting guesses for the auxiliary variables and the model parameters to be adjusted.

Furthermore, the critical line that delimits the Stg phase can be cast in a form similar to the equation that determines the spinodals associated with the first-order transitions,

$$\hat{\kappa}_2\, e^{2k} + \hat{\kappa}_1 e^{k} + \hat{\kappa}_0 = 0, \tag{A15}$$

$$\begin{aligned}\hat{\kappa}_2 = {} & [(z-1)q - z]\{[ze^{2j} - e^{-2j}(z-2)](q^2 - m^2) \\ & + e^{\ell}(q+m)^2 + e^{-\ell}(q-m)^2\},\end{aligned} \tag{A16}$$

$$\begin{aligned}\hat{\kappa}_1 = {} & e^{j}(1-q)\{e^{\ell}(q+m)[(z^2-1)q - m(z-1)^2 - 2z] \\ & + e^{-\ell}(q-m)[(z^2-1)q + m(z-1)^2 - 2z] \\ & + 2e^{-2j}[m^2(z-1)^2 - (z-3)(z-1)q^2 - 2q]\},\end{aligned} \tag{A17}$$

$$\hat{\kappa}_0 = 4(1-q)^2[(z-1)q - 1]. \tag{A18}$$

APPENDIX B: BIPARTITE-LATTICE EQUATIONS

In this Appendix, we provide the equations obtained by considering a formulation of the problem on a bipartite lattice, with two interpenetrating sublattices labeled a and b.

The recurrence relations for the truncated pseudoaverages read

$$m_n^a = \frac{e^{h_a} X^{z-1}\left(m_{n+1}^b, q_{n+1}^b\right) - \omega e^{h_a}\, Y^{z-1}\left(m_{n+1}^b, q_{n+1}^b\right)}{e^{-\mu_a} + e^{h_a} X^{z-1}\left(m_{n+1}^b, q_{n+1}^b\right) + \omega e^{h_a}\, Y^{z-1}\left(m_{n+1}^b, q_{n+1}^b\right)}, \tag{B1}$$

$$q_n^a = \frac{e^{h_a} X^{z-1}\left(m_{n+1}^b, q_{n+1}^b\right) + \omega e^{h_a}\, Y^{z-1}\left(m_{n+1}^b, q_{n+1}^b\right)}{e^{-\mu_a} + e^{h_a} X^{z-1}\left(m_{n+1}^b, q_{n+1}^b\right) + \omega e^{h_a}\, Y^{z-1}\left(m_{n+1}^b, q_{n+1}^b\right)}, \tag{B2}$$

$$m_{n-1}^b = \frac{e^{h_b} X^{z-1}\left(m_n^a, q_n^a\right) - \omega e^{h_b}\, Y^{z-1}\left(m_n^a, q_n^a\right)}{e^{-\mu_b} + e^{h_b} X^{z-1}\left(m_n^a, q_n^a\right) + \omega e^{h_b}\, Y^{z-1}\left(m_n^a, q_n^a\right)}, \tag{B3}$$

$$q_{n-1}^b = \frac{e^{h_b} X^{z-1}\left(m_n^a, q_n^a\right) + \omega e^{h_b}\, Y^{z-1}\left(m_n^a, q_n^a\right)}{e^{-\mu_b} + e^{h_b} X^{z-1}\left(m_n^a, q_n^a\right) + \omega e^{-h_b}\, Y^{z-1}\left(m_n^a, q_n^a\right)}, \tag{B4}$$

with the functions $X(m,q)$ and $Y(m,q)$ being the same as those of the uniform case. The BL grand-potential density per site is given by

$$\begin{aligned}\beta\psi = {} & \tfrac{1}{2}\ln(1-q_a) + \tfrac{1}{2}\ln(1-q_b) + \tfrac{1}{2}(z-2)\ln\big[1 - q_a q_b + \tfrac{1}{4}e^{j+k+\ell}(q_a+m_a)(q_b+m_b) \\ & + \tfrac{1}{4}e^{j+k-\ell}(q_a-m_a)(q_b-m_b) + \tfrac{1}{2}e^{k-j}(q_a q_b - m_a m_b)\big].\end{aligned} \tag{B5}$$

Finally, the order parameters on the BL, thermodynamically conjugated to the fields (h_a, h_b, μ_a, μ_b), read

$$\begin{aligned}m_a^0 = {} & -2\left(\frac{\partial\beta\psi}{\partial h_a}\right)_{h_b,\mu_a,\mu_b} \\ = {} & \frac{4m_a(1-q_b) + e^{j+k+\ell}(q_a+m_a)(q_b+m_b) - e^{j+k-\ell}(q_a-m_a)(q_b-m_b) + 2e^{k-j}(m_a q_b - m_b q_a)}{4(1-q_a q_b) + e^{j+k+\ell}(q_a+m_a)(q_b+m_b) + e^{j+k-\ell}(q_a-m_a)(q_b-m_b) + 2e^{k-j}(q_a q_b - m_a m_b)},\end{aligned} \tag{B6}$$

$$\begin{aligned}m_b^0 = {} & -2\left(\frac{\partial\beta\psi}{\partial h_b}\right)_{h_a,\mu_a,\mu_b} \\ = {} & \frac{4m_b(1-q_a) + e^{j+k+\ell}(q_a+m_a)(q_b+m_b) - e^{j+k-\ell}(q_a-m_a)(q_b-m_b) - 2e^{k-j}(m_a q_b - m_b q_a)}{4(1-q_a q_b) + e^{j+k+\ell}(q_a+m_a)(q_b+m_b) + e^{j+k-\ell}(q_a-m_a)(q_b-m_b) + 2e^{k-j}(q_a q_b - m_a m_b)},\end{aligned} \tag{B7}$$

$$\begin{aligned}q_a^0 = {} & -2\left(\frac{\partial\beta\psi}{\partial \mu_a}\right)_{h_a,h_b,\mu_b} \\ = {} & \frac{4q_a(1-q_b) + e^{j+k+\ell}(q_a+m_a)(q_b+m_b) + e^{j+k-\ell}(q_a-m_a)(q_b-m_b) + 2e^{k-j}(q_a q_b - m_a m_b)}{4(1-q_a q_b) + e^{j+k+\ell}(q_a+m_a)(q_b+m_b) + e^{j+k-\ell}(q_a-m_a)(q_b-m_b) + 2e^{k-j}(q_a q_b - m_a m_b)},\end{aligned} \tag{B8}$$

$$\begin{aligned}q_b^0 = {} & -2\left(\frac{\partial\beta\psi}{\partial \mu_b}\right)_{h_a,h_b,\mu_a} \\ = {} & \frac{4q_b(1-q_a) + e^{j+k+\ell}(q_a+m_a)(q_b+m_b) + e^{j+k-\ell}(q_a-m_a)(q_b-m_b) + 2e^{k-j}(q_a q_b - m_a m_b)}{4(1-q_a q_b) + e^{j+k+\ell}(q_a+m_a)(q_b+m_b) + e^{j+k-\ell}(q_a-m_a)(q_b-m_b) + 2e^{k-j}(q_a q_b - m_a m_b)}.\end{aligned} \tag{B9}$$

As it should be, one regains the uniform-case BL order parameters, Eqs. (30) and (31), by simply dropping the sublattice labels a and b from the equations.

APPENDIX C: MODEL PARAMETERS AND POSSIBLE TYPES OF PHASE DIAGRAMS

In this Appendix, we obtain the conditions relating the model parameters that define the possible types of phase diagrams. In the Appendix of Ref. [23] the authors mapped the three asymptotic limiting models that describe the G-LE, G-LC, and LE-LC first-order transitions into the spin-1/2 Ising model. According to this analysis, and extending their results to the $\bar{h} \neq 0$ case, the representative values $(\bar{\mu}_1, \bar{\mu}_2, t_1, t_2)$ displayed in Fig. 2 could be estimated by

$$\frac{\bar{\mu}_1}{z} = \frac{\bar{h}}{z} - \frac{1}{2}(1 + \bar{k} - \bar{\ell})\left[1 + \frac{1}{2}\phi(z)\ln\omega\right],$$
$$\frac{\bar{\mu}_2}{z} = -\frac{\bar{h}}{z} - \frac{1}{2}(1 + \bar{k} + \bar{\ell}), \tag{C1}$$

$$\frac{t_1}{z} = \frac{1}{4}(1 + \bar{k} - \bar{\ell})\phi(z), \quad \frac{t_2}{z} = \frac{1}{\ln\omega}\left(\bar{\ell} + \frac{2\bar{h}}{z}\right), \tag{C2}$$

with $\phi(z)$ given by Eq. (43). The corresponding MFA coordinates [23] can be obtained by taking the infinity-coordination limit $\phi(z \to \infty) \to 1$, whereas for Monte Carlo calculations one should replace the exact t_c^{exact} in the definition of $\phi(z) \to t_c^{\text{exact}}/t_c^{\text{MFA}}$.

However, besides the standard uniform (G, LE, LC) phases, we have found a staggered (Stg) phase for some set of parameters $(\bar{k}, \bar{\ell}, \omega, z)$, which requires a formulation of the problem on a bipartite lattice for a proper treatment. In fact, in Ref. [23], the authors overlooked that, for $\bar{\ell} > 1 + \bar{k}$, the estimated G-LE line critical temperature becomes negative, $t_1 < 0$, which implies that the effective spin-1/2 Ising model for the G-LE transition becomes *antiferromagnetic*. Therefore, the reasoning that yields the estimated temperature t_3 must be based on results of the spin-1/2 *antiferromagnetic* Ising model, which displays a *critical line* on the $H \times T$ plane. We define the correction factor for the antiferromagnetic case,

$$\phi^-(\tilde{h}, z) \equiv \frac{t_c^{\text{BPA}}(\tilde{h}, z)}{t_c^{\text{MFA}}(\tilde{h}, z)}, \tag{C3}$$

which now depends on the effective magnetic field $\tilde{h}$. Therefore, under the condition $\bar{\ell} > 1 + \bar{k}$, Eqs. (A7), (A12), and (A13) of Ref. [23], which define a first-order line ending at a critical point, should be replaced by equations describing a whole critical line $(\mu_c, t_c, \tilde{h}_c)$,

$$\frac{\tilde{h}}{z} = -\frac{1}{4}(\bar{\ell} - 1 - \bar{k}) + \frac{1}{2z}(\bar{\mu} - \bar{h}) + \frac{t}{2z}\ln\omega, \tag{C4}$$

$$\frac{\bar{\mu}_c}{z} = \frac{\bar{h}}{z} + \frac{2\tilde{h}_c}{z} + \frac{1}{2}(\bar{\ell} - 1 - \bar{k})\left[1 - \frac{1}{2}\phi^-(\tilde{h}_c, z)\ln\omega\right], \tag{C5}$$

$$\frac{t_c}{z} = \frac{1}{4}(\bar{\ell} - 1 - \bar{k})\phi^-(\tilde{h}_c, z), \tag{C6}$$

which is consistent with the lobe geometry that bounds the Stg phase on the $t \times \bar{\mu}$ phase diagrams of types (e) and (f), shown in Fig. 2. For bipartite lattices and at the MFA and BPA levels, the Néel temperature defined for $\tilde{h}_c = 0$ coincides with the critical temperature of the associated spin-1/2 ferromagnetic Ising model,

$$\phi^-(\tilde{h}_c = 0, z) = \phi(z), \tag{C7}$$

and we are able to obtain estimates for the chemical potential $\bar{\mu}_3$ and temperature t_3,

$$\frac{\bar{\mu}_3}{z} \equiv \frac{\bar{\mu}_c}{z}(\tilde{h}_c = 0) = \frac{\bar{h}}{z} + \frac{1}{2}(\bar{\ell} - 1 - \bar{k})\left[1 - \frac{1}{2}\phi(z)\ln\omega\right]$$
$$= \frac{\bar{\mu}_1}{z} - \frac{1}{2}(\bar{\ell} - 1 - \bar{k})\phi(z)\ln\omega, \tag{C8}$$

$$\frac{t_3}{z} \equiv \frac{t_c}{z}(\tilde{h}_c = 0) = \frac{1}{4}(\bar{\ell} - 1 - \bar{k})\phi(z) = -\frac{t_1}{z}. \tag{C9}$$

As discussed in the Appendix of Ref. [23], the approximated conditions for occurrence of the G-LE critical point (and the associated first-order line) and the existence of a critical point along the LE-LC first-order line can be cast in terms of two inequalities involving the parameter $\bar{\ell}$,

$$\exists \text{ G-LE critical point if } t_1 > t_2 \;\rightarrow\; \bar{\ell} < \frac{1 + \bar{k}}{1 + \frac{4}{\phi(z)\ln\omega}} - \frac{2\bar{h}}{z}\left[1 + \frac{1}{4}\phi(z)\ln\omega\right]^{-1} \equiv \bar{\ell}_+(\bar{k}), \tag{C10}$$

$$\exists \text{ LE-LC critical point if } t_2 > t_c^{\text{BPA}} \;\rightarrow\; \bar{\ell} > \phi(z)\ln\omega - \frac{2\bar{h}}{z} \equiv \bar{\ell}_0. \tag{C11}$$

Although the Stg phase was overlooked in Ref. [23]—as their MFA analysis was solely based on uniform ferromagnetic phases—one may also consider the approximated condition $t_3 = |t_1| > t_2$ as related to its onset,

$$\exists \text{ Stg phase if } t_3 = |t_1| > t_2 \;\rightarrow\; \bar{\ell} > \frac{1 + \bar{k}}{1 - \frac{4}{\phi(z)\ln\omega}} - \frac{2\bar{h}}{z}\left[1 - \frac{1}{4}\phi(z)\ln\omega\right]^{-1} \equiv \bar{\ell}_-(\bar{k}). \tag{C12}$$

Table II summarizes the possible combinations of the three conditions, Eqs. (C10), (C11), and (C12), as well as their relation to the different types of phase diagrams shown in Fig. 2 for $\bar{h} = 0$. An explicit representation, on the plane $(\bar{\ell}, \bar{k})$, of the conditions of Table II for $\bar{h} = 0$ is given in Fig. 7 for three different sets of the parameters (z, ω). The first set ($z = 4$, $\omega = 10^3$) corresponds to the values chosen in Ref. [23] to perform their numerical calculations, while the remaining

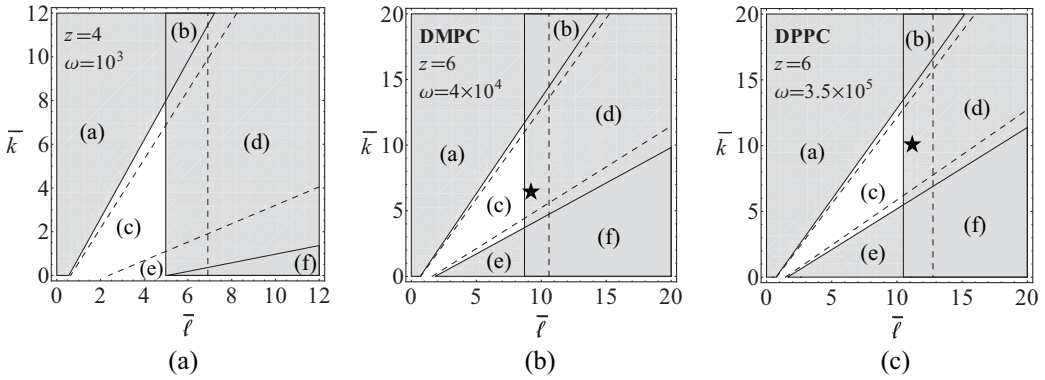

FIG. 7. Conditions on the $(\bar{\ell}, \bar{k})$ plane defined by Eqs. (C10), (C11), and (C12), for $\bar{h} = 0$ and some set of parameters (z, ω): (a) values chosen for numerical calculations in Ref. [23]; (b) values corresponding to DMPC; (c) values corresponding to DPPC. Solid lines correspond to the BPA results, while the dashed lines are obtained under MFA by taking $\phi(z) \to 1$. The labels on the different regions are associated with the possible topologies of phase diagrams shown in Fig. 2 and also listed in Table II. The symbols (★) indicate the parameters found by fitting experimental data of the mentioned lipids to theoretical BPA results [28]: DMPC ($\bar{\ell} = 9.30161$, $\bar{k} = 6.51200$), and DPPC ($\bar{\ell} = 11.17619$, $\bar{k} = 10.20970$).

two sets correspond to the values chosen in Ref. [28] to characterize two specific zwitterionic phospholipids, DMPC ($z = 6$, $\omega = 4 \times 10^4$) and DPPC ($z = 6$, $\omega = 3.5 \times 10^5$). In principle, any phase-diagram topology displayed in Fig. 2 could be obtained by varying the parameters $(\bar{\ell}, \bar{k})$, but their adjusted values to experimental data [28], shown in Fig. 7 by symbols (★), laid both in the (d)-type region, presenting thus just a first-order line ending at a LE-LC critical point. It is interesting that the parameters $(\bar{\ell}, \bar{k})$ found by fitting are close to the border between the phase diagrams of types (c) and (d) of Fig. 2, which differ by the presence of a critical point that ends the LE-LC first-order transition line.

TABLE II. Possible $\bar{h} = 0$ phase-diagrams topologies—as labeled in Fig. 2—and conditions for the occurrence of the G-LE and LE-LC critical points (CPs) and the Stg phase.

Type	Conditions on $\bar{\ell}$	G-LE CP	LE-LC CP	Stg phase
a	$\bar{\ell} < \bar{\ell}_0 \wedge \bar{\ell} < \bar{\ell}_+(\bar{k})$	√	×	×
b	$\bar{\ell} > \bar{\ell}_0 \wedge \bar{\ell} < \bar{\ell}_+(\bar{k})$	√	√	×
c	$\bar{\ell} < \bar{\ell}_0 \wedge \bar{\ell} < \bar{\ell}_-(\bar{k}) \wedge \bar{\ell} > \bar{\ell}_+(\bar{k})$	×	×	×
d	$\bar{\ell} > \bar{\ell}_0 \wedge \bar{\ell} < \bar{\ell}_-(\bar{k}) \wedge \bar{\ell} > \bar{\ell}_+(\bar{k})$	×	√	×
e	$\bar{\ell} < \bar{\ell}_0 \wedge \bar{\ell} > \bar{\ell}_-(\bar{k})$	×	×	√
f	$\bar{\ell} > \bar{\ell}_0 \wedge \bar{\ell} > \bar{\ell}_-(\bar{k})$	×	√	√

[1] O. G. Mouritsen, *Life—As a Matter of Fat: The Emerging Science of Lipidomics*, The Frontiers Collection (Springer-Verlag, Berlin, 2005), Chap. 2, p. 24.
[2] S. J. Singer and G. L. Nicolson, Science **175**, 720 (1972).
[3] V. M. Kaganer, H. Möhwald, and P. Dutta, Rev. Mod. Phys. **71**, 779 (1999).
[4] D. E. Gragson, D. Beaman, and R. Porter, J. Chem. Educ. **85**, 272 (2008).
[5] Y. F. Hifeda and G. W. Rayfield, Langmuir **8**, 197 (1992).
[6] N. R. Pallas and B. A. Pethica, Langmuir **9**, 361 (1993).
[7] N. Denicourt, P. Tancrède, and J. Teissié, Biophys. Chem. **49**, 153 (1994).
[8] L. R. Arriaga, I. López-Montero, J. Ignés-Mullol, and F. Monroy, J. Phys. Chem. B **114**, 4509 (2010).
[9] K. Y. C. Lee, Annu. Rev. Phys. Chem. **59**, 771 (2008).
[10] O. G. Mouritsen, Chem. Phys. Lipids **57**, 179 (1991).
[11] B. Myer, E. Evans, and O. G. Mouritsen, Q. Rev. Biophys. **24**, 293 (1991).
[12] J. F. Nagle, J. Chem. Phys. **58**, 252 (1973).
[13] S. Doniach, J. Chem. Phys. **68**, 4912 (1978).
[14] E. Ising, Z. Phys. **31**, 253 (1925).
[15] L. Onsager, Phys. Rev. **65**, 117 (1944).
[16] C. N. Yang, Phys. Rev. **85**, 808 (1952).
[17] T. D. Lee and C. N. Yang, Phys. Rev. **87**, 410 (1952).
[18] A. Caillé, D. Pink, F. de Verteuil, and M. J. Zuckermann, Can. J. Phys. **58**, 581 (1980).
[19] M. J. Zuckermann and D. Pink, J. Chem. Phys. **73**, 2919 (1980).
[20] O. G. Mouritsen, A. Boothroyd, R. Harris, N. Jan, T. Lookman, L. MacDonald, D. A. Pink, and M. J. Zuckermann, J. Chem. Phys. **79**, 2027 (1983).
[21] M. N. Tamashiro, C. Barbetta, R. Germano, and V. B. Henriques, Phys. Rev. E **84**, 031909 (2011).
[22] V. B. Henriques, R. Germano, M. T. Lamy, and M. N. Tamashiro, Langmuir **27**, 13130 (2011).
[23] H. S. Guidi and V. B. Henriques, Phys. Rev. E **90**, 052705 (2014).
[24] D. Mukamel and M. Blume, Phys. Rev. A **10**, 610 (1974).
[25] J. Sivardière and J. Lajzerowicz, Phys. Rev. A **11**, 2101 (1975).
[26] P. D. Gujrati, Phys. Rev. Lett. **74**, 809 (1995).
[27] L. K. Nielsen, T. Bjørnholm, and O. G. Mouritsen, Langmuir **23**, 11684 (2007).
[28] F. O. de Oliveira and M. N. Tamashiro, Phase transitions in phospholipid monolayers: theory versus experiments, 10.1021/acs.langmuir.8b03244.
[29] M. Blume, V. J. Emery, and R. B. Griffiths, Phys. Rev. A **4**, 1071 (1971).

[30] J. Lajzerowicz and J. Sivardière, Phys. Rev. A **11**, 2079 (1975).
[31] J. Sivardière and J. Lajzerowicz, Phys. Rev. A **11**, 2090 (1975).
[32] J. F. Baret and J. L. Firpo, J. Colloid Interface Sci. **94**, 487 (1983).
[33] J. P. Legré, J. L. Firpo, and G. Albinet, Phys. Rev. A **31**, 1703 (1985).
[34] M. Banville, A. Caillé, and G. Albinet, J. Phys. (France) **46**, 101 (1985).
[35] A. Pękalski, Eur. Biophys. J. **16**, 39 (1988).
[36] C. Buzano and L. R. Evangelista, J. Phys.: Condens. Matter **6**, 5323 (1994).
[37] D. A. Lavis and G. M. Bell, *Statistical Mechanics of Lattice Systems*, Vol. 1: Closed-form and Exact Solutions (Springer-Verlag, Berlin, 1999), Sec. 7.4, pp. 181–187.
[38] C. J. Thompson, J. Stat. Phys. **27**, 441 (1982).
[39] R. J. Baxter, *Exactly Solved Models in Statistical Mechanics*, 3rd printing, Dover Books on Physics Series (Dover, Mineola/NY, 2007), Chap. 4, pp. 47–59.
[40] L. K. Runnels, J. Math. Phys. **8**, 2081 (1967).
[41] T. P. Eggarter, Phys. Rev. B **9**, 2989 (1974).
[42] E. Müller-Hartmann and J. Zittartz, Phys. Rev. Lett. **33**, 893 (1974).
[43] M. Ostilli, Phys. A **391**, 3417 (2012).
[44] K. Huang, *Statistical Mechanics*, 2nd ed. (Wiley, New York, 1987), Sec. 14.5, pp. 357–361.
[45] R. K. Pathria, *Statistical Mechanics*, 2nd ed. (Butterworth-Heinemann, Oxford, 1996), Sec. 11.6, pp. 328–334.
[46] D. A. Lavis and G. M. Bell, *Statistical Mechanics of Lattice Systems*, Vol. 1: Closed-form and Exact Solutions (Springer-Verlag, Berlin, 1999), Sec. 7.3, pp. 178–181.
[47] S. R. A. Salinas, *Introduction to Statistical Physics* (Springer-Verlag, New York, 2001), Sec. 13.4, pp. 268–271.
[48] A. Ercule and M. N. Tamashiro, Phys. Rev. E **97**, 062145 (2018).
[49] J. T. Bartis, J. Chem. Phys. **59**, 5423 (1973).
[50] R. J. Baxter, *Exactly Solved Models in Statistical Mechanics*, 3rd printing, Dover Books on Physics Series (Dover, Mineola/NY, 2007), Chap. 6, pp. 72–87.
[51] G. H. Wannier, Phys. Rev. **79**, 357 (1950).
[52] G. H. Wannier, Phys. Rev. B **7**, 5017 (1973).
[53] R. M. F. Houtappel, Physica **16**, 425 (1950).
[54] C. Domb, Adv. Phys. **9**, 245 (1960).
[55] M. N. Tamashiro and S. R. Salinas, Phys. Rev. B **56**, 8241 (1997).
[56] A. Pelizzola and M. Pretti, Phys. Rev. B **60**, 10134 (1999).
[57] X. Qian, M. Wegewijs, and H. W. J. Blöte, Phys. Rev. E **69**, 036127 (2004).
[58] Y. Han, Y. Shokef, A. M. Alsayed, P. Yunker, T. C. Lubensky, and A. G. Yodh, Nature **456**, 898 (2008).
[59] E. Jurčišinová, M. Jurčišin, and A. Bobák, Phys. Lett. A **378**, 1448 (2014).
[60] K. A. Riske, R. P. Barroso, C. C. Vequi-Suplicy, R. Germano, V. B. Henriques, and M. T. Lamy, Biochim. Biophys. Acta (Biomembranes) **1788**, 954 (2009).
[61] S. Doniach, J. Chem. Phys. **70**, 4587 (1979).
[62] M. Marder, H. L. Frisch, J. S. Langer, and H. M. McConnell, Proc. Natl. Acad. Sci. U.S.A. **81**, 6559 (1984).
[63] J. M. Carlson and J. P. Sethna, Phys. Rev. A **36**, 3359 (1987).
[64] W. S. McCullough and H. L. Scott, Phys. Rev. Lett. **65**, 931 (1990).
[65] G. Cevc, Biochim. Biophys. Acta (Biomembranes) **1062**, 59 (1991).
[66] T. C. Lubensky and F. C. MacKintosh, Phys. Rev. Lett. **71**, 1565 (1993).
[67] S. Kirchner and G. Cevc, Europhys. Lett. **28**, 31 (1994).
[68] W.-J. Sun, S. Tristram-Nagle, R. M. Suter, and J. F. Nagle, Proc. Natl. Acad. Sci. U.S.A. **93**, 7008 (1996).
[69] M. F. Schneider, D. Marsh, W. Jahn, B. Kloesgen, and T. Heimburg, Proc. Natl. Acad. Sci. U.S.A. **96**, 14312 (1999).
[70] T. Heimburg, Biophys. J. **78**, 1154 (2000).